Materials Science & Engineering C 121 (2021) 111829

Contents lists available at ScienceDirect

Materials Science & Engineering C

journal homepage: www.elsevier.com/locate/msec

A novel multifunctional NCQDs-based injectable self-crosslinking and in situ forming hydrogel as an innovative stimuli responsive smart drug delivery system for cancer therapy

S. Türk [a,b], I. Altınsoy [c], G. Çelebi Efe [d], M. Ipek [c], M. Özacar [b,e], C. Bindal [c,*]

[a] Sakarya University, Biomedical, Magnetic and Semi Conductive Materials Research Center (BIMAS-RC), Esentepe Campus, 54187, Sakarya, Turkey
[b] Biomaterials, Energy, Photocatalysis, Enzyme Technology, Nano & Advanced Materials, Additive Manufacturing, Environmental Applications and Sustainably Research & Development Group (BIOENAMS R&D Group), 54187, Sakarya, Turkey
[c] Sakarya University, Faculty of Engineering, Department of Metallurgy and Materials Engineering, Esentepe Campus, 54187, Sakarya, Turkey
[d] Sakarya University of Applied Sciences, Faculty of Technology Metallurgical and Materials Engineering, Esentepe Campus, 54187, Sakarya, Turkey
[e] Sakarya University, Science & Arts Faculty, Department of Chemistry, Sakarya 54187, Turkey

ARTICLE INFO

Keywords:
NCQDs
Hydroxyapatite
Smart drug delivery
Stimuli responsive

ABSTRACT

In this work, we offer an easy approach to develop a novel injectable, pH sensitive and in situ smart drug delivery system for use in cancer treatments. The developed hydrogels containing nitrogen doped carbon quantum dots (NCQD), doxorubicin (Dox) and hydroxyapatite (HA) were obtained by in situ self-crosslinking. Characterization of the synthesized nanomaterials, interactions between NCQD/Dox/HA hydrogel structure were carried out by TEM, FESEM, EDS, FTIR, XPS, XRD, Zeta potential, DLS, UV–Vis, SEM, gelation time, injectability and DIST measurements. In addition, antibacterial evaluation which was performed against *Staphylococcus aureus* realized that HA compound significantly increased the antibacterial activity of the hybrid hydrogel. The anticancer drug release to the tumor cell microenvironment with a pH of 5.5 was found to be higher compared to the release in the normal physiological range of pH 6.5 and 7.4. MTT and live/dead assays were also performed using L929 fibroblastic cell lines to investigate the cytotoxic behavior of NCQDs, and NCQDs/Dox/HA hydrogels. Furthermore, the NCQDs/Dox/HA hydrogel could transport Dox within a MCF-7 cancerous cell at specifically acidic pH. Additionally, imaging of cell line was observed using NCQDs and their use in imaging applications and multicolor features in the living cell system were evaluated. The overall study showed that in situ formed NCQDs/Dox/HA hydrogel represented a novel and multifunctional smart injectable controlled-release drug delivery system with great potential, which may be considered as an attractive minimal invasive smart material for future intelligent delivery of chemotherapeutic drug and disease therapy applications.

1. Introduction

Cancer is one of the most common causes of human death worldwide and can cause 13.2 million deaths by 2030 [1,2]. The most common and widely used clinical treatments include systemic intravenous administration of chemotherapeutic agents. However, conventional chemotherapy agents have tremendous disadvantages, as they damage normal cells in addition to tumor cells, because they have side effects and both short and long term toxic risks. Therefore, chemotherapy often causes an unsatisfactory healing effect due to the low therapeutic efficacy of drugs and their side effects on healthy tissues.

Doxorubicin (Dox) is one of the most widely used anticancer chemotherapeutics and is a broad spectrum anti-cancer drug, shows excellent therapeutic efficacy in several types of cancers [3,4]. However, intravenous chemotherapy of free Dox often causes systemic toxicity and serious complications such as cardio toxicity, typhlitis, myelosuppression, nausea, vomiting and alopecia, which inhibits its clinic applications [5,6]. Therefore, to minimize toxic side effects and increase anticancer efficacy, developing various effective delivery systems for Dox is really a matter of urgency.

In recent years, the development of stimuli-responsive multifunctional smart anti-cancer drug delivery systems (MSDDS) attracted great attention in biomedicine and this scope will greatly expand [7–9]. The therapeutic nanostructured MSDDS with many advantages comparing

* Corresponding author.
E-mail address: bindal@sakarya.edu.tr (C. Bindal).

https://doi.org/10.1016/j.msec.2020.111829
Received 19 September 2020; Received in revised form 8 December 2020; Accepted 20 December 2020
Available online 2 January 2021

with the traditional dosage forms play a significant role in numerous biomedical applications such as multi-imaging and treatment of different types of cancers [10]. The creation of stimulating sensitive controlled-release smart systems for targeted drug delivery is very important in cancer treatment. In particular, the pH-sensitive smart drug delivery system is of great interest due to the more acidic microenvironments of extra- and intra-cancerous cells (pH 4.0–7.0) compared to normal cells microenvironments (i.e. 7.4) [11]. The smart drug delivery system should prevent or reduce the side effect caused by the drug bursting from drug carriers in the design of drug release because the burst release drug can be absorbed in a short time and accumulate in both metabolic organs and adjacent tissues. An ideal MSDDS should also have the following features in addition to the above: excellent biocompatibility, tunable properties, facile synthesis of compounds and favorable system type such as injectable in-situ gelling hydrogel [12]. However, the need for a system that combines these features remains a big challenge in this field until now. In this juncture, the current research demands a next generation drug delivery systems with combined these features for overcoming this challenge.

Nitrogen doped into carbon quantum dots (CQDs) provide improved efficiency, create additional functionalities on the surface of CQDs outside the carbon core such as more active additional linking groups to easily conjugate with molecules, showed much better performance than CQDs and thus nitrogen doped carbon quantum dots (NCQDs) continues to draw increasing attention in recent years by many research groups around the world as the next generation of multifunctional nanomedicine research area [13,14] . NCQDs is still at its infant stage, scientists have been inspired to exert more efforts to endow them with the innovative design, more functions, unprecedented possibilities, broaden their uses [15,16].

Hydroxyapatite, [HA, $Ca_{10}(PO_4)_6(OH)_2$] has recently attracted a great deal interest in design of drug delivery systems due to its excellent properties such as nontoxicity to biosystems, ability to carry drugs by conjugating interactions, containing –OH groups, having numerous different binding sites (i.e. negatively charged P regions and positively charged Ca regions on its surface) capacity to penetrate the cell membranes [17,18]. Further, HA is pH sensitive and under moderate acidic conditions (like during the resorption by osteoclasts or inside a cell in a lysosome), phosphorous and calcium elements can decompose from the HA surface [19,20]. These ions can be excreted or metabolized by the cell without any side effects [21]. In order to achieve prolonged the drug releasing time, pH sensitive smart drug delivery system without the leakage of drug, we suggest that HA can be used as component in efficient in situ gelling hydrogel type drug delivery systems which may represent a novel approach, formed with appropriate interactions.

In this study, we aimed to develop pH sensitive and injectable NCQDs/HA/Dox multifunctional intelligent hydrogel, can be created in situ, with innovative design with externally activated release of Dox for cancer treatment. NCQDs simply reacted with HA and Dox via Schiff base, hydrogen bonding and ionic interactions, yielding multiple opportunities to easily produce this multicomponent hydrogel (Scheme 1). Both dynamic chemical and physical interactions under physiological conditions are used to form stable hydrogel via self-crosslinking without harmful release by products and use of extra cross-linking agents.

To the best of our knowledge, this smart drug delivery system (in situ gelling NCQDs/Dox/HA) with multi-functional features is presented in first time. Furthermore, the information of dynamic Schiff Base chemical bonding between NCQDs and Dox molecules is an important feature for pH sensitivity, in-situ forming smart NCQDs based hydrogel.

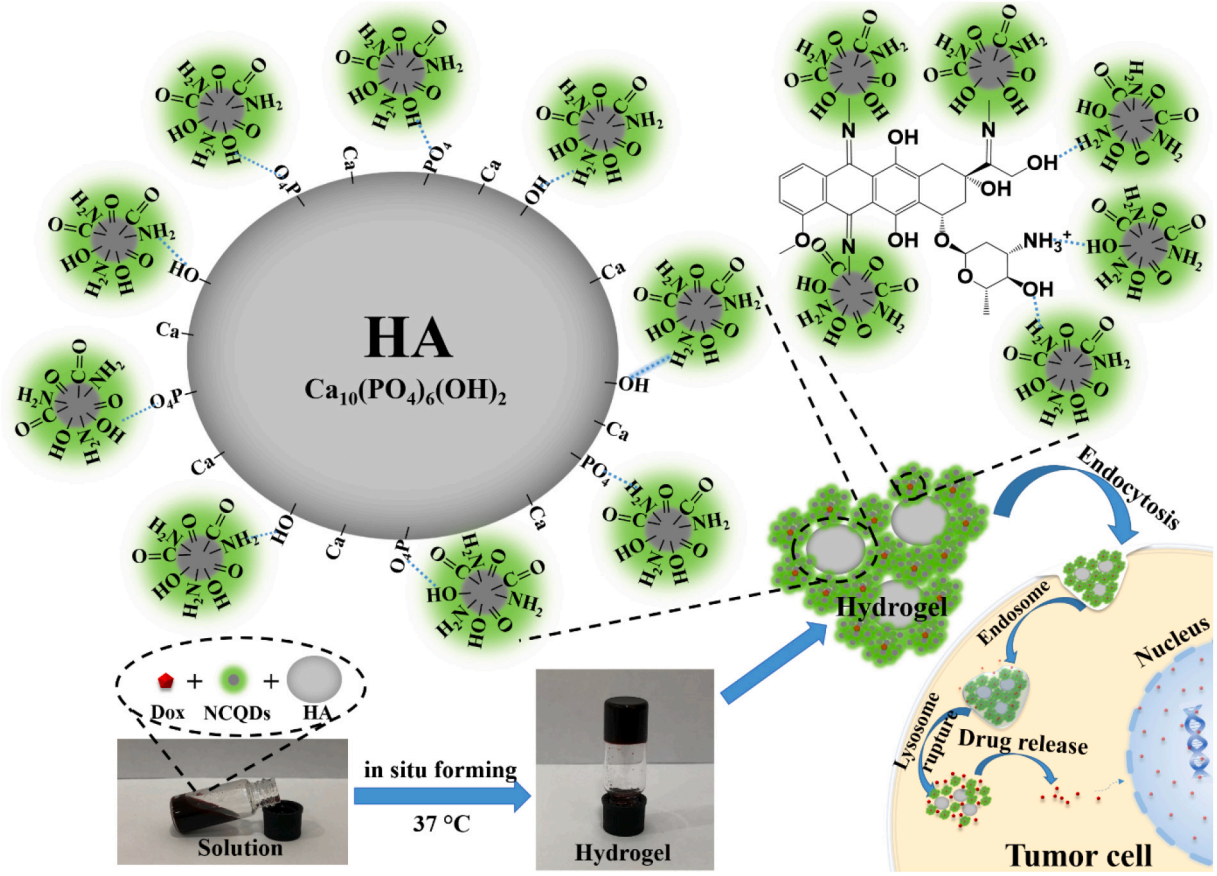

Scheme 1. Schematic illustration for the multifunctional NCQDs/Dox/HA hybrid hydrogel formed in-situ with the possible self-crosslinking chemical interactions, and the tumor cell triggered release mechanism.

2. Experimental section

Experimental details about the preparation processes and characterization techniques used in this study can be found in the supporting information.

2.1. Statistical analysis

The means and standard deviations of data were calculated. Data were presented as the mean ± standard deviation (SD). Differences between groups were analyzed by one-way analysis of variance (ANOVA, Tukey test). The level of the statistical significance is given by *p*-values ($^{*}p < 0.05$, $^{**}p < 0.01$ and $^{***}p < 0.001$) calculated by using Origin software (Origin Lab Corporations). p values less than 0.05 were considered statistically significant.

3. Results and discussion

3.1. Characterization and properties of synthesized powders and prepared hydrogels

The morphology and size of the synthesized NCQDs were examined using Transmission Electron Microscope (TEM). The results were given in the supporting information as Fig. S1, demonstrate that the NCQDs regularly formed with spherical shaped morphology and well dispersed in aqueous solutions with a lateral size of less than 10 nm which can be clearly distinguishable. Fig. S1a also indicated that no agglomeration occurred during the synthesis of the NCQDs. Fig. S1b was a representative the size distribution (the histogram), which was obtained from TEM images by statistical analysis obeying a Gaussian distribution. It can be claimed that the diameters of synthesized NCQDs in the picture was in the range of 4–6 nm with an average diameter of ~4.89 nm as calculated from the size distribution, which confirms the homogeneous and relatively narrow size distribution of monodispersed as-prepared NCQDs on TEM grid. The calculated results similar to that fabricated from Glucose [22] and Citric acid [23] but much smaller than that of fabricated from Silk (ca. 62 nm) [24]. Since the Dynamic Light Scattering (DLS) analysis measures the total hydrodynamic size of the particles, this value was also consistent with the size obtained from the DLS analysis. The morphology and elemental analysis of HA nanoparticles were characterized by Field Emission Scanning Electron Microscope (FESEM) and Energy Dispersive Spectroscopy (EDS), which were depicted in Fig. S1c and d, respectively. FESEM images of pure HA nanoparticles depicted that uniform irregular or spherical shaped HA nanoparticles were successfully yielded and the average size of Nano-HA was found to be about in range of 60–100 nm which was also consistent with the DLS results. Elemental composition analysis of HA nanoparticles showed that HA consisted of only calcium (Ca), phosphorus (P), oxygen (O) elements and the ratio of Ca/P was found to be 1.59 (Fig. S1d). These results concluded that the HA nanoparticles were successfully synthesized.

Fourier Transform Infrared (FTIR) spectra were performed to verify the surface functional groups of NCQDs, NCQDs/Dox, NCQDs/Dox/HA, HA and the results were presented in Fig. S2a. The wt/vol ratios of the components in the all experimental sample groups were listed in Supplementary information (Table S1). Significant peaks of pure HA nanoparticles were observed at 890–1180 and 490–610 cm^{-1} which were associated with the phosphate (PO_4) group internal vibrations. These vibrations belong to the asymmetric stretching, bending mode and antisymmetric stretching vibrations of tetrahedral PO_4. For the NCQD spectrum, the broad absorption peak at around 3405 cm^{-1} was assigned to the O–H and N–H asymmetric stretching modes. The peaks at about 2800–2900 cm^{-1} were attributed to –CH groups. The peaks at 1720 cm^{-1} and 1640 cm^{-1} corresponded to C═O and C═C stretching vibrations, respectively. Specifically, the small broad bands at 1456 cm^{-1}, 1152 cm^{-1} and 1097 cm^{-1} indicated the vibrations of C–N groups in NCQDs [22]. These results showed that there are various nitrogen and oxygen containing functional groups including $–NH_2$, –OH and –COOH on the surface of the NCQDs. In the FTIR spectrum of NCQDs/Dox sample, the observed peak at 1230 cm^{-1} were attributed to C−O (epoxide). The reason why this peak is smaller than that of NCQDs/Dox/HA is thought to be due to ionic interactions between Ca^{2+} and epoxide and entanglement of epoxide groups with HA due to Ca^{2+} in HA. FTIR spectrum of NCQDs/Dox showed an absorption band at 1680 cm−1 corresponding to the C═N group, which indicates occurrence of the Schiff's base reaction. A small symmetrical vibration band for the NCQDs aldehyde group at around 1720 cm^{-1} disappeared due to formation of covalent bonding to form a Schiff base, which was existed as an absorption band at around 1680 cm^{-1} [25].

The crystal structures and phase compositions of HA, NCQDs, NCQDs/Dox and NCQDs/Dox/HA were analyzed by X-ray Diffraction (XRD) and presented in Fig. S2b. As it can be seen from Fig. S2b, the peaks at $2\theta = 10.91°$, 25.86°, 28.41°, 31.77°, 32.91°, 34.11°, 39.79°, 46.66°, 49.45°, 64.09° and 77.08° indicated characteristic peak positions of HA, which were related to the diffracting plane (101), (002), (210), (211), (300), (202), (301), (222), (213), (304) and (513) of HA, respectively. It can be claimed that all the diffraction peaks of synthesized HA were well indexed to the lattice plane of standard HA (JCPDS No. 009-0432) [26]. None of the peaks belonging to $CaCO_3$ or $Ca_3(PO_4)_2$ can be found, which showed that the synthesized HA was single phase. Additionally, the XRD pattern of the as-prepared NCQDs showed an obvious broad diffraction peak centered at around 20.14°, which demonstrates the existence of the amorphous phase of NCQDs have the 0.44 nm lattice spacing of the (002) diffraction peak belonging to NCQDs [27]. This wide peak due to highly disordered carbon atoms was attributed to the introduction of nitrogen- and oxygen- containing groups or surface defects on the NCQD structure. There was no statistically significant difference in the diffraction peaks between NCQDs and NCQDs/Dox. The absence of the sharp peaks in NCQDs/Dox pattern indicated that Dox was well distributed and encapsulated in amorphous forms in NCQDs/Dox successfully. The XRD pattern of NCQDs/Dox/HA was similar to that of synthesized HA except a peak at 21.67° due to the characteristic peak of NCQDs. The XRD pattern of HA had a small shift to higher angles probably because of the slightly reduced d-spacing and accumulation of NCQDs on the HA nanoparticles. The lattice spacing also changed from 0.44 to 0.43 and 0.41 nm for NCQDs/Dox and NCQDs/Dox/HA, respectively. Lattice narrowing in this range was common for nanoscale materials, which was probably expanded rich active sites on the surface of NCQDs by the possible covalent bonds between NCQDs/Dox and NCQDs/HA. The diffraction peaks of HA in conjugated NCQDs/Dox/HA become weaker than those of pure HA, which indicates that the crystallinity of the HA was impaired by the NCQDs and Dox on the nano-HA surface.

To investigate the surface functional groups of the NCQDs, NCQDs/Dox and NCQDs/Dox/HA, X-ray Photoelectron Spectroscopy (XPS) analyzes were carried out and the results of core level spectra (high resolution XPS spectra of the C 1s, N 1s, O 1s, Ca 2p and P 2p region) were depicted in Fig. S3a–j. The mixture of Gauss and Lorentzian peaks were utilized to fit core levels and least square iterative program was used for fitting. The survey spectrum in Fig. S3a showed peaks of C1s at 284.8 eV, N1s at 399.2 eV and O1s at 531.2 eV demonstrating NCQDs consist of the elements C, N and O. Quantitative determination by XPS showed that the surface atomic concentration of C, N and O was found as 67.97%, 16.39% and 15.68%, respectively, and this demonstrated the successful introduction of nitrogen. High resolution scanning of the C 1s, N 1s and O 1s regions were demonstrated in Fig. S3b-d. The C 1 s spectrum of NCQDs indicated three main components and these correspond to C=C or C–C at ca. 284.88 eV, C–N at ca. 286.00 eV, and C=O or C=N at ca. 288.2 eV [28]. This result showed that the synthesized N-doped CQDs were rich in hydroxyl and carboxyl groups on the surface, which was compatible with the FT-IR spectrum.

The binding energy detected at peak of 286.00 eV implied the

existence of amide groups which was in agreement with the results of FTIR. In addition, the XPS N 1 s spectrum of the NCQDs in Fig. S3c exhibited two deconvoluted peaks at about 399.1 eV and 400.8 eV confirming the presence of the nitrogen atoms of pyridinic-like, and pyrrolic-like [28], respectively. This result implied that nitrogen was bounded to carbon through the covalent binding.

The high-resolution O 1s spectrum of NCQDs (Fig. S3d) suggested three bonding peaks at a binding energy of 530.8 eV, 531.9 eV and 533.1 eV, indicating the existence of O−H, C−O and C=O [29], respectively. These XPS results indicated that NCQDs were rich in oxygen and nitrogen atoms. The XPS data of survey and C1s, N1s core level spectra obtained for NCQDs/Dox were presented in Fig. S3e–g. In NCQDs/Dox system, the peaks at 284.72 eV and 286.6 eV referred to the –C=C/C–C and –C–N or –C–O–C–bonds of Dox [30] with slight shift, respectively. N 1 s peaks appearing at 399.3, 397.7 and 395.3, corresponded to pyridinic-like, pyrrolic-like and the formation of −N=N− bond, respectively, and it demonstrated the presence of various nitrogen. Due to the binding of Dox to NCQDs by transfer of electron density, it can be expected that the peak position of N 1s decreased by several eVs. The C 1s of NCQDs/Dox was also deconvoluted with three peaks. Compared with NCQDs (Fig. S3b), the intensity of C−C/C=C and C−N/C−O−C of NCQDs/Dox significantly increased, which is due to rich carbon–carbon bonds and carbon–oxygen-carbon of the Dox molecule. It should be noted that the elemental analysis of NCQDs/Dox reveals the increase of the atomic percentage of carbon and decrease of nitrogen as compared to that of NCQDs. These results were due to the nitrogen ratio of NCQDs was higher than Dox molecules. In Fig. S3g, additional peaks were observed at 134 eV and 347 eV, which corresponded to P 2p, Ca 2p binding energy values of HA, respectively. XPS analysis was also performed to determine the ratio of phosphate and calcium ions belonging to the NCQDs/Dox/HA hybrid surface. The peak corresponding to 2p calcium and phosphorus orbitals was used to determine Ca/P ratio on surface of NCQDs/Dox/HA calculated by using the area under the corresponding elementary peak in the high resolution XPS spectrum. The Ca/P ratio was 1.61, which close to the theoretical Ca/P ratio for HA of 1.67. The individual spectra for Ca and P for NCQDs/Dox/HA sample was presented in Fig. S3 h-i. The high-resolution of Ca 2p spectrum deconvoluted into two peaks $2p_{1/2}$ and 2p3/2 at 351.0 and 347.1 eV [31], respectively, were related to calcium phase on HA. It was understood from the peak seen around 347.3 eV associated with $Ca2p_{3/2}$ that calcium atoms were bound to phosphate groups (PO_4^{3-}). In Fig. S3i, high-resolution P 2p spectrum can also be deconvoluted into two peaks with a spin orbit splitting for $2p_{1/2}$ and $2p_{3/2}$ levels with binding energies 134.5 eV and 133.3 eV [32], respectively. The peaks in all these Ca and P spectra were characteristic of the HA oxidation states (Ca^{2+} and P^{5+}). In addition, zeta potential, DLS and UV–Visible absorption measurements of the NCQDs and NCQDs/Dox, and NCQDs/Dox/HA conjugates were made for the characterization and detailed explanations together with the relevant figure (Fig. S5) were given in the supporting information.

The interior morphology of the lyophilized and vertically cut off hydrogel was characterized by SEM as shown in Fig. 1. Cross-sectional morphologies of the hydrogels, prepared through lyophilization of a self-assembled hybrid hydrogel formed by an in-situ hydrogelation at 37 °C, revealed that the fabricated gels have different surface morphologies. SEM analysis was carried to understand the external porous structure of the cross-sectional prepared NCQDs (Fig. 1a-b), NCQDs/Dox

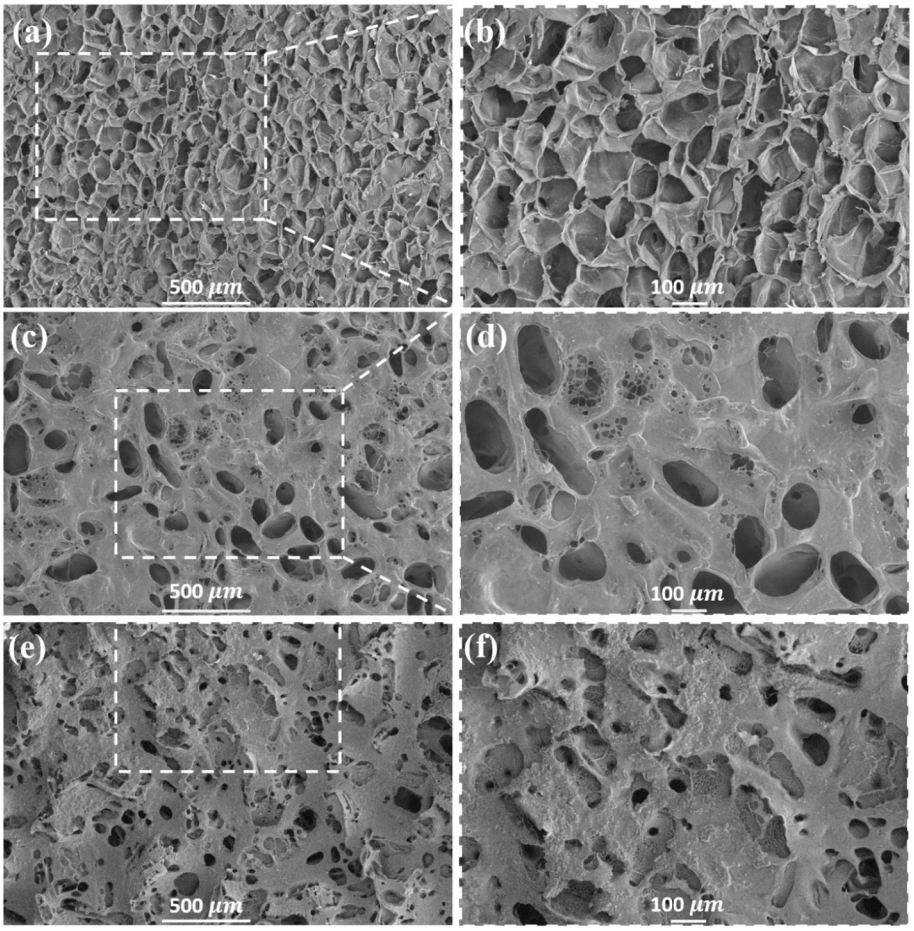

Fig. 1. Morphology of lyophilized hydrogels: SEM images of (a-b) NCQDs (0.6 wt/vol), (c-d) NCQDs/Dox (0.6/0.2 wt/vol) and (e-f) NCQDs/Dox/HA (0.6/0.2/0.2 wt/vol) hydrogels.

(Fig. 1c-d) and NCQDs/Dox/HA (Fig. 1e-f) and all hydrogels exhibited continuous three-dimensional structure interconnected with micron-sized porosities, where the pores were the result of ice crystal formation during the lyophilization process. This interconnected highly internal channel systems are an essential parameter for facilitate cell adhesion, proliferation; oxygen and nutrient transportation as well as metabolic waste diffusion [33]. The introduction of physical and chemical cross-linking which occurred through the electrostatic interactions, hydrogen bindings and Schiff base reactions were owing to the existence of a large number of oxygen-containing functional groups and bonding between $-NH_2$ and $-CHO$, which are believed to be responsible for producing the 3-D network structure. The NCQDs and NCQDs/Dox/HA showed spherically shaped pores with mean diameter in the range of 20−150 μm and 20−50 μm, respectively. On the contrary, irregular porous structures with pore size in the range of 1−200 μm were observed in the NCQDs/Dox. The SEM micrograph of the NCQDs hydrogels (Fig. 1a-b) showed the uniform distributed and coherent pores, although the small sized NCQDs were not clearly visible from the micrographs. The uniform distribution of NCQDs within the NCQDs/Dox/HA hydrogel network was clearly observed from the elemental mapping (Fig. S4). SEM images of the NCQDs/Dox hydrogels exhibited that the pore size increased slightly with addition of Dox in the NCQDs/Dox hydrogel due to an increase in the number of hydrophilic moieties in the hydrogels and these images of NCQDs/Dox hydrogel confirmed Dox binding to NCQDs. The obtained NCQDs/Dox/HA was superior to other NCQDs based hydrogels previously reported [34] due to its regular porosity. Stronger binding capacity of Dox to the NCQD network is important to facilitate sustained release of the drug. After the addition of HA, good microporous structures without structural deterioration were observed on SEM images (Fig. 1e-f). The average hydrogel pore size decreased by the addition of HA, which can be induced by the higher crosslinking density of the hydrogel and it was expected to increase the number of ice crystal nucleation sites. These results also indicated that the porosity and cross-sectional morphology of the hydrogel network can be adjusted by changing the amount of HA and Dox to NCQDs. The homogeneous distribution of HA at nanometer scale in the hydrogels can also be observed from the high-magnification SEM image (Fig. 1f) without agglomeration, similar to those reported in reference [35]. Further observation at high magnification (x100) demonstrated that there were many HA particles between of pores and it leaded to enhance the exterior surface roughness which was in contrast to smooth exterior surface in NCQDs and NCQDs/Dox hydrogels (Fig. 1a-b and c-d). The incorporation of HA in NCQDs/Dox gels made the internal structure slightly rougher than NCQDs and NCQDs/Dox hydrogels. HA was uniformly dispersed within the NCQDs/Dox without obvious aggregation, in accordance with the results of elemental mapping (Fig. S4).

In order to fabricate 3D gel structure, Dox and HA were added to NCQDs solution. The gelation of hybrid NCQDs solutions occurred at 7.4 pH and 37 °C, human physiological pH condition for practical use of an injectable hydrogel to the human body, without any external intervention. Changes in the hydrogel solution may alter the gelling time of NCQDs. To evaluate how Dox and HA change the gelling time of the NCQD hydrogel, a vial inversion test method was performed [36]. The gelation time of NCQDs, NCQDs/Dox and NCQDs/Dox/HA solutions differed according to the introduction of components as shown in Fig. 2. NCQDs solution without any Dox or HA was gelled after 121 s. However, it was measured that the gelation time of NCQD solutions was reduced by adding both Dox and Dox/HA (Fig. 2).

An increase in weight/volume percentage (% wt/vol) of NCQDs concentrations within groups of NCQDs-1 (0.4% wt/vol), NCQDs-2 (0.6% wt/vol) and NCQDs-3 (0.8% wt/vol) caused a reduction in gelation time. Likewise, the decrease in gelation time observed in NCQDs/Dox and NCQDs/Dox/HA with increasing concentration of Dox [NCQDs/Dox-1 (0.6%/0.1% wt/vol), NCQDs/Dox-2 (0.6%/0.2% wt/vol) and NCQDs/Dox-3 (0.6%/0.4% wt/vol)] or HA [NCQDs/Dox/HA-1

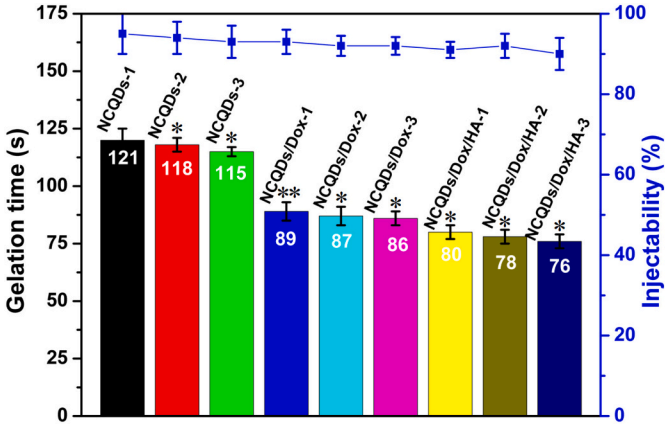

Fig. 2. Gelation times (via inverting method) and injectability (via commercial disposable syringes) of NCQDs (0.6 wt/vol), NCQDs/Dox (0.6/0.2 wt/vol) and NCQDs/Dox/HA (0.6/0.2/0.2 wt/vol) combinations. $*p < 0.05$ and $**p < 0.01$, and indicated significant differences after each addition.

(0.6%/0.2%/0.1% wt/vol), NCQDs/Dox/HA-2 (0.6%/0.2%/0.2% wt/vol) and NCQDs/Dox/HA-3 (0.6%/0.2%/0.2% wt/vol)] (Fig. 2). In the case of only presence of NCQDs, self-assembly was conducted by H− bonding interactions [37]. Abundant carboxylic acid and amino groups on the surface of NCQDs could form H-bond interactions between NCQDs-NCQDs and NCQDs-solvent and gelation may have occurred when the interactions between the latter two were very weak. Further stabilization may resulted from other interactions that include bridges between NCQDs−NCQDs, such as dense H− bonds, and also increased the concentration of NCQDs and the number of reactive groups per unit volume, which supports the importance of H− bonds for gel formation. The slight decrease in gelation times seen in NCQDs groups (NCQDs-1, NCQDs-2 and NCQDs-3), NCQDs/Dox groups (NCQDs/Dox-1, NCQDs/Dox-2 and NCQDs/Dox-3) and NCQDs/Dox/HA groups (NCQDs/Dox/HA-1, NCQDs/Dox/HA-2 and NCQDs/Dox/HA-3) was not statistically significant when compared to the reduced gelation time in transition between NCQDs with NCQDs/Dox. It was obvious that adding Dox into NCQDs hydrogels significantly reduced the gelation time. In the case of hybrid hydrogel obtaining, it is important for the NCQDs participating both the formation of H− bonds and Schiff base reaction. Gelation time tests confirmed that Dox were responsible for decreasing gelation time of NCQDs/Dox due to conjugation between NCQDs and Dox, which was also confirmed by FTIR and XPS results. Similarly, the gelation behavior of Dox conjugated NCQD gel gelation was close to gelation of Dox and HA loaded gel, suggesting that Dox interaction was predominant in drug conjugated NCQD gels.

HA particles in NCQDs/Dox/HA solution may have interacted with NCQDs and Dox molecules, which led to faster assembly of Dox conjugated NCQDs. The gelation time of NCQDs/Dox/HA ranged from 80 s to 76 s and could be easily adjusted by addition of component, which would be beneficial for further clinical application. HA and NCQDs were hydrophilic materials with responsible for active groups such as hydroxyl and carboxyl groups that can form hydrogen bonds with Dox conjugated NCQDs. Addition of HA in the hydrogel resulted in a faster gelation and decreasing porosity (as can be seen from the Fig. 1). These results were in accordance with those obtained in reference [38]. Such rapid gelling will lead to greater retention of the drug in the formed hydrogel and hence a slower drug release pattern. As a result, we suggested that the carboxylic and amino groups present on the NCQDs surface favor H− bond, Schiff base reaction, which is effective in the gelling time as reported in reference [39], and cationic−anionic interactions among NCQDs, Dox, and HA. The NCQDs hydrogels prepared by both physical (H bonds, hydrophilic, and electrostatic interactions) and chemical in situ crosslinking (Schiff-base reaction between NCQDs and Dox) without harmful release of by products and using of extra

cross-linking agents.

Fig. 2 also presented the injectability of NCQDs, NCQDs/Dox and NCQDs/Dox/HA combinations. The injectability of NCQDs hybrid hydrogel was only slightly decreased as addition of Dox and HA, similar to those obtained in reference [38], while injectability increased with reduced CaP content. In the view of injectability at different gelation time, there was no remarkable difference between hydrogels and adding Dox and HA did not affect the high injectability of NCQD hydrogels. Injectability of all the prepared hydrogel was found between 95% and 90% without any filter pressing, which allowed drug delivery in vivo in a minimally invasive clinical application with NCQDs/Dox/HA in situ hydrogel, resulted in less pain and a smaller scar size for patients.

The dynamic interfacial surface tension (DST) curves of the NCQD solution with different concentrations at pH 6.0 were shown in Fig. 3(a), where the adsorption kinetics were similar and the difference at the interface tension values was due to different interface tensions of air/water. While NCQDs were rapidly adsorbed within 1000 s despite surface hydrophilicity, the adsorption equilibrium time remained almost constant by increasing concentration of NCQD. Also, long-term DST decreased with increasing NCQD concentration. The decrease in surface tension with increasing NCQDs concentration was similar to the adsorption behavior of NCQDs in graphene oxide solution [40] and adsorption behavior of 16Ser/8–8Ser surfactant used for Dox delivery [41].

The effects of Dox on the DST of NCQDs solution at pH of 6.0 and 4.3 were shown in Fig. 3 (b) and (e). DST curves at both pH 6.0 and 4.3 of the NCQDs/Dox mixture were found to be similar to those of the pure NCQD solution after adding a small amount of Dox. Moreover, the Schiff base reaction was favorable for the formation of NCQDs/Dox complex and also addition of Dox to NCQDs would reduce the charge repulsion between NCQDs. As can be seen from the results, Dox in its low concentration caused a decrease in DST and therefore had an important effect on the adsorption behavior of NCQDs. As a result, the NCQDs/Dox complex dominated the surface adsorption layer, and the similarity observed between the two interfaces both at pH 6.0 and 4.3 which means to be similar to the adsorption phenomenon. The kinetics of adsorption, which is time to achieve meso-equilibrium tension, decreased with the addition of Dox. It can be acclaimed that, increasing time was thought to be the reason for the increase in volume due to the fact that Dox was surrounded by NCQDs, thus the diffusion coefficient of hybrid was reducing, which was directly affected by the size and consistent with the results of hydrodynamic diameter (Fig. S5b.).

In Fig. 3 c and f, adding a small amount of HA did not affect NCQDs/Dox formation, and the adsorption properties of NCQDs/Dox remained almost unchanged. As the HA content increased further, it was observed that the surface tension decreased and thus a gradual increase in the adsorption rate of NCQD/Dox/HA. This result was different from the effects of HA on the surface tension on Span 80 [42]. The NCQDs/Dox/HA hybrid has been absorbed at interface more slowly than the other solutions, the time required to achieve meso-equilibrium and adsorption kinetics noticeably slowed down from 200 to about 400 s with the addition of HA. This case was thought to be the reason for the increase in volume due to the NCQDs/Dox was wrapped around the HA, thus decreasing the diffusion coefficient of hybrid was observed. The increased duration was directly affected by the size and consistent with results in the hydrodynamic diameter [43], which can be attributed to the interaction of NCQDs with HA. Hence, NCQDs that were smaller than NCQDs/Dox or NCQDs/Dox/HA diffused faster and reached the balance earlier. HA had hydrophilic hydroxyl groups on its surface and NCQDs were adsorbed onto HA nanoparticle surfaces, thus it formed hydrogen bonds. In addition, hybrid complex formation can be considered for the interaction mechanism between nanoparticles, since the probability of collision at a higher HA concentration would increase and thus the formation of the NCQDs/Dox/HA hybrid complex will be supported.

As shown in Fig. 3 d, e and f, the effects of Dox and HA on the DST of NCQDs solution at pH 4.3 differed from the results obtained at pH 6.0. The mesoequilibrium surface tension of all prepared hybrid solutions decreased compared with the corresponding results at pH 4.3. NCQD molecules were positively charged when the pH of the environment where the surface located was lower than the isoelectric point. Electrostatic attraction between Dox and NCQDs molecules, which are oppositely charged, affected the dynamic adsorption properties and supported the formation of the NCQDs/Dox hybrid. The formation of

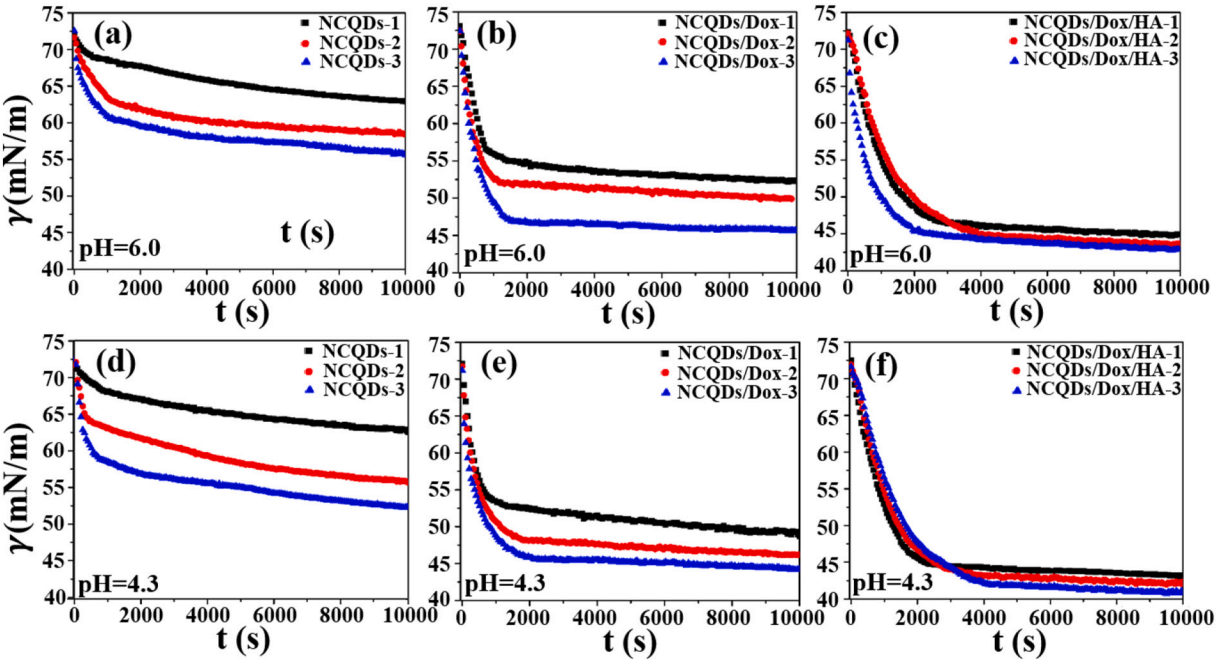

Fig. 3. Time-dependent Dynamic interfacial surface tension measurements (via pendant drop method) of (a) and (d) NCQDs solution at pH 6.0 and 4.3, respectively; (b) and (e) NCQDs/Dox (0.6/0.2 wt/vol) solution at pH 6.0 and 4.3, respectively; (c) and (f) NCQDs/Dox/HA (0.6/0.2/0.2 wt/vol) solution at pH 6.0 and 4.3, respectively.

NCQDs/Dox or NCQDs/Dox/HA hybrids maintained electrostatic repulsion between NCQDs molecules, thereby reducing the barrier of electrostatic adsorption. As a result, hybrid formation at pH 4.3 slightly increased the adsorption rate on the interface surface, enhanced surface activity and reduced DST.

The reduction in interfacial tension for each sample from the initial value can be attributed to progressive adsorption of hybrids to the interface. For the additions of NCQDs, Dox and HA at both 6.0 and 4.3 pH, the surface tension of NCQDs solution was slightly higher than that of the NCQDs/Dox solution, similarly that of the NCQDs/Dox solution was higher than that of the NCQDs/Dox/HA solution. This showed that NCQD, Dox and HA have a synergistic effect on reducing surface tension and that NCQDs interacted with Dox and HA. It was estimated that, as prepared NCQDs/Dox/HA smart drug delivery system, consisting of surface-active complex in solution, exploited a self-regulation mechanism arising from noncovalent attraction between NCQDs−NCQDs; and dynamic covalent Schiff base reaction between NCQDs−Dox; and ionic attractions between NCQDs/Dox−HA in order to develop simple but effective hybrid NCQDs surrounded by Dox and HA component. It was thought that this NCQDs/Dox/HA nano-sized smart drug carrier system can increase the effectiveness of drugs, reduce toxicity by increasing biomembrane permeability (due to the size is appropriate for to pass into the cell and surrounded by NCQDs to facilitate passage into the cell as shown in Fig.S5b) and improve bioavailability (due to the binding was not used and components is biocompatible).

In the in vitro antibacterial experiment, which is important in drug delivery [44,45], disc diffusion method was used to investigate the antibacterial activity of HA, NCQDs, NCQDs/Dox and NCQDs/Dox/HA, which were investigated as a potential new antibacterial drug delivery system (Fig. 4). The same amount of powdered samples on agar plates contain HA (Fig. 4a), NCQDs (Fig. 4b), NCQDs/Dox (Fig. 4c) and NCQDs/Dox/HA (Fig. 4d).

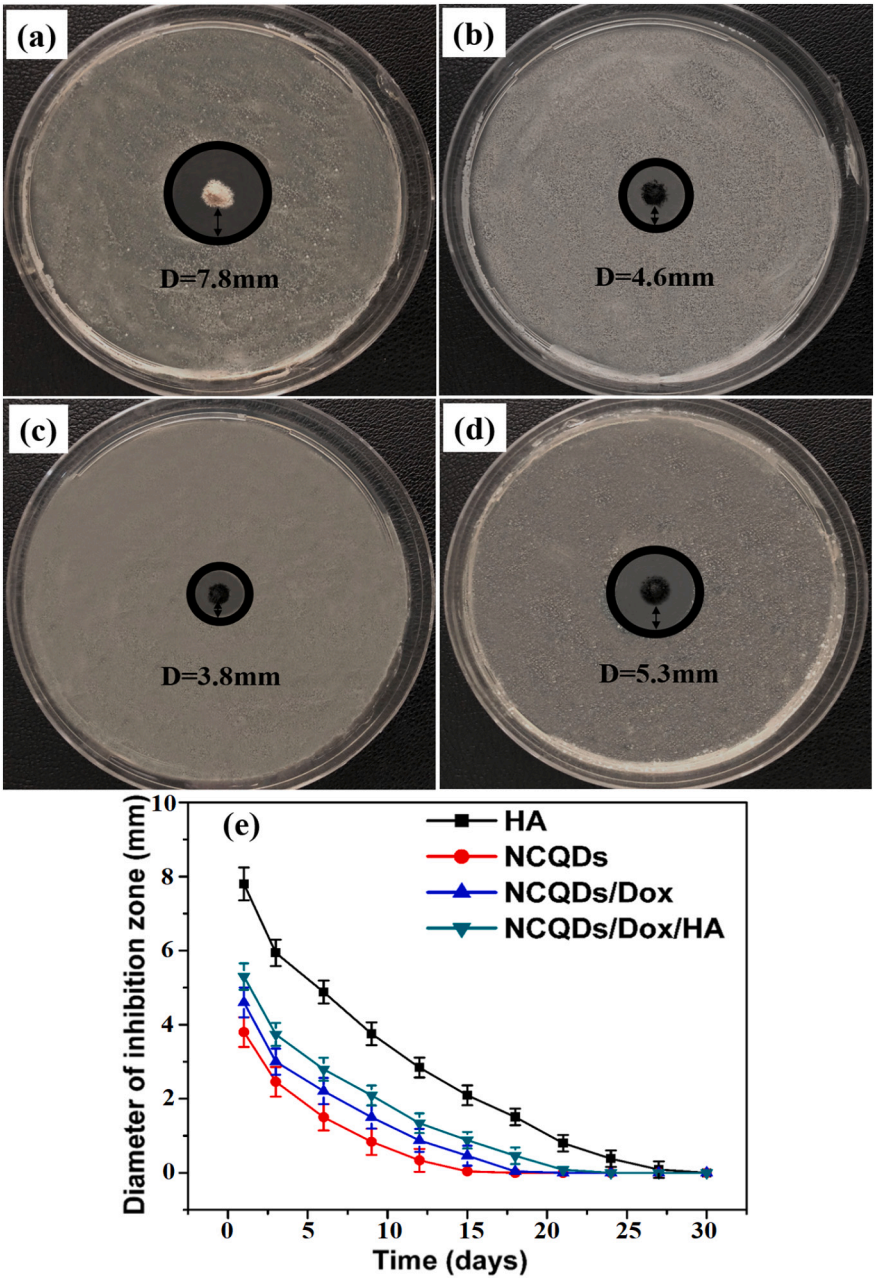

Fig. 4. Antibacterial activity (via disk diffusion method) of (a) HA, (b) NCQDs, (c) NCQDs/Dox (0.6/0.2 wt.) and (d) NCQDs/Dox/HA (0.6/0.2/0.2 wt) against *S. aureus* bacteria on agar plate. (e) Changes in inhibition zone values of HA, NCQDs, NCQDs/Dox (0.6/0.2 wt.) and NCQDs/Dox/HA (0.6/0.2/0.2 wt) versus time.

In this study, *Staphylococcus aureus* (*S. aureus*) was chosen as a model organism because it is a common Gram positive pathogen that can cause various diseases such as skin infections, sepsis, bloodstream infections and pneumonia. Obvious inhibition zones for HA, NCQDs, NCQDs/Dox and NCQDs/Dox/HA were observed on the agar plates (Fig. 4). The inhibition zones of HA, NCQDs, NCQDs/Dox and NCQDs/Dox/HA were 7.8, 4.6, 3.8 and 5.3 mm on average, respectively. HA has been found to have the most antibacterial effect (Fig. 7a, D = 7.8 mm) compared to other examples. The presence of Ca^{2+} mineral in the synthesized HA may have results in antibacterial activity as reported in literature [46]. NCQDs showed antibacterial effect against *S. aureus* and its inhibitions zone was found to be 4.6 mm as shown in Fig. 4b. Compared to pure NCQD (Fig. 4b), no increase in the inhibition zone of NCQDs/Dox (Fig. 4c) hybrid has been found, indicating that equal amounts of substrates have antibacterial effect on *S. aureus* bacteria, but Dox addition reduced bacterial activity. This may be attributed to the reduction in the amount of NCQDs in NCQDs/Dox sample compared to pure NCQDs sample. The antibacterial properties of the obtained NCQDs were compatible with several recent studies [22,47]. The increase of the inhibition zone from 3.8 to 5.3 mm with the addition of HA (Fig. 4c and d) showed that introduction of HA into the hydrogels by either chemical bonding or physical incorporation can result in hydrogels with enhanced antimicrobial activity. These results also confirmed that the NCQDs/Dox/HA could be successfully used as good antibacterial to prevent bacterial infection during the clinical injections.

The variation of the diameter of inhibition zone was determined according to different materials in *S. aureus* changes over time, and it was found that the maximal inhibition zone values of the materials were obtained at 24 h incubation, and then decreased with time (Fig. 4e). Nonetheless, the antibacterial activities as measured by the inhibition zone of NCQDs/Dox/HA exerted on *S. aureus* lasted 23 days, longer than the samples without HA added, indicating the NCQDs/Dox/HA hybrid may have the most potent bactericidal effect, compared with the pure NCQDs and NCQDs/Dox hybrid samples. Our results were comparable to the reported data in the literature. Therefore, such low cost NCQDs/Dox/HA hybrids with strong and prolonged antimicrobial activity are expected to have great potential in clinical applications.

3.2. *pH-sensitive drug delivery, cytotoxicity and multicolor cellular bioimaging studies*

The potential application of NCQDs/Dox and NCQDs/Dox/HA hydrogels for smart drug delivery was evaluated by examining the drug releases in vitro from these hydrogel at physiological temperature 37 °C which was plotted in Fig. 5a and b, respectively. At different pH environment, the release behavior varied. Sustained release of the drug in two hydrogels was observed in the buffer solutions at pH 7.4, 6.5, 5.5 and 4.0 up to 72 h to find out if there is the ability to selectively release more drugs in the cancer area. Since the early release of Dox will have a toxic effect for normal cells, it is important that drug release occurs only when the target area is reached for successful implementation of smart drug delivery systems [48]. Evaluating the pH-sensitive drug release behavior of drug delivery systems was essential to minimize the toxicity of the drug to normal tissues, as it can interact with different cells with varying pH values in the body. In this study, we adjusted the release environments with pH of 6.5 and 7.4 to simulate the extracellular pH (pH = 5.7–7.8) of tumor and normal tissues, respectively. In addition, we examined the pH-dependent release behavior at lower pH values (at pH 5.5) since the pH of the intra-tumor endosomal is 5.5−6.0.

The cumulative drug release behavior of the drug from both hydrogels was slow and continues with a two-stage release profile, a first rapid release, and a relatively slow next release at all values of pH. The release rate of Dox in NCQDs/Dox was faster than that of Dox in NCQDs/Dox/HA, and more obviously influenced by the pH of the environment for both hydrogels. The results confirmed that Dox in the NCQDs/Dox/HA was well incorporated in the hydrogels and connections of Dox in the

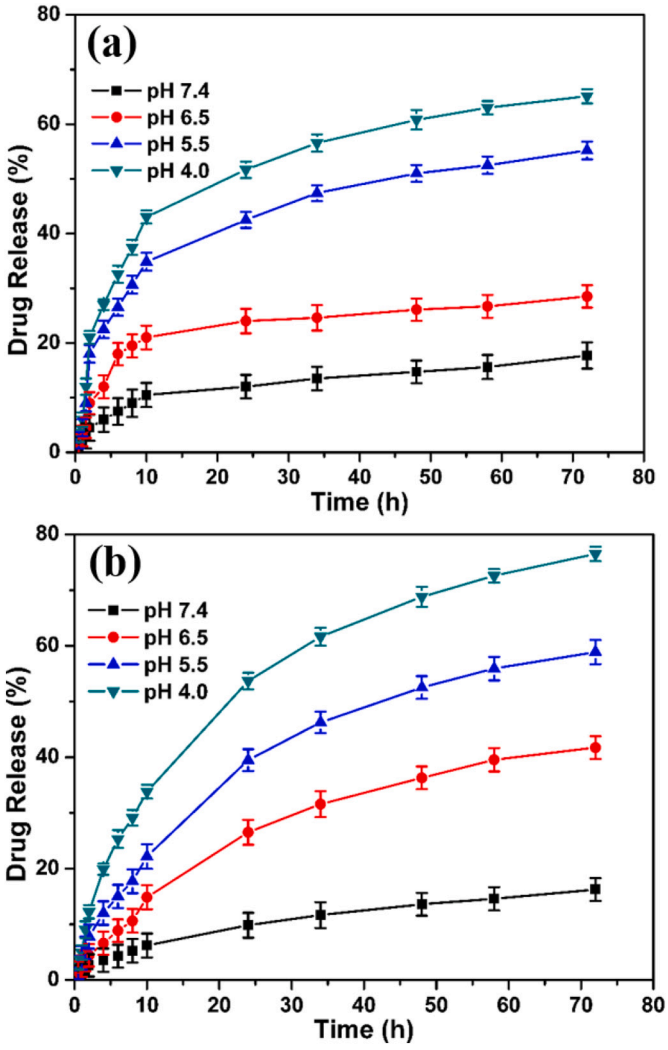

Fig. 5. In vitro release of Dox (via UV–Vis spectrophotometry method) form the (a) NCQDs/Dox (0.6/0.2 wt/vol) and (b) NCQDs/Dox/HA (0.6/0.2/0.2 wt/vol) hydrogels in buffers at pH values of 7.4, 6.5, 5.5 and 4.0.

NCQDs/Dox/HA hydrogel have increased compared with in NCQDs/Dox hydrogel. The in vitro drug release in both two hydrogels can be accelerated simultaneously by lowering the ambient pH from 7.4 to 6.5, 5.5 and 4.0 due to the dynamically reversible Schiff base bonds between Dox and NCQDs, which are stable at physiological pH and unstable at acidic pH. Moreover, the hydrogen-bonding interaction between NCQDs, Dox and HA was the strongest at pH 7, resulting in an inefficient release, while hydrogen bonding interactions weakened under acid condition. The acid-sensitive binder with pH of 6.5 was a weak acid environment where it will break at a lower rate, and this was a dynamic reversible reaction unless too much water can be removed in this weak environment. At pH of 5.5 and especially 4.0, a high release profile was observed due to a faster fracture rate of the bond, indicating that hydrogels had a high rate of acid-sensitive Dox release.

As shown in Fig. 5a and b, the Dox release increased from 17% to 65% for NCQDs/Dox and from 16% to 74% for NCQDs/Dox/HA with pH decreasing from 7.4 to 4.0, respectively. In addition to pH-sensitive disintegration of the Schiff base bond, the dissolution of HA [49] can help release the loaded drug in acidic conditions, which weakens the interaction between HA nanoparticles and Dox. The initial burst release of Dox from NCQDs/Dox was relatively observed comparison with the NCQDs/Dox/HA hydrogel in which release period was continued without initial burst release. The percentage of Dox release from the

NCQDs/Dox/HA hydrogel was only 15% after 72 h of incubation in buffer solution at pH 7.4, suggesting that the NCQDs/Dox/HA hydrogel could prevent drug burst release and increase the drug's reach to tumor tissue. In the current hydrogel system, drugs loaded in NCQDs-based hydrogels can be released by weakening or breaking down dynamic Schiff-based bonds and ionic interactions in hydrogels due to protonated and positively charged amino groups at acidic pH. Significantly more Dox was released from prepared pH sensitive smart hydrogels around cancerous tissues than normal tissue, which reduced side effects for normal tissue and increased drug efficiency to kill tumor cells [50]. Compared to the previous results [51], where HA based Dox delivery systems also demonstrated enhanced release of DOX in acidic conditions, the release after 72 h was lower in the present study, which can be attributed to the highly self-crosslinked hydrogel network by bonding between NCQDs and Dox. The pH-dependent drug release from NCQDs/Dox/HA could be exploited for smart target drug delivery applications and will afford active drug release from NCQDs/Dox/HA smart delivery vehicles.

MTT assay, where lower absorbance means higher cell inhibition rate, shows the cell inhibition rate of prepared samples. In Fig. 6a, MCF-7 being a breast cancer cell line cells revealed similar viability of tissue culture plates (TCPs) used as controls with NCQDs/Dox and NCQDs/Dox/HA hydrogels at pH 7.4 for 24 h. Dox released from NCQDs/Dox/HA hydrogel after 24 h at pH 7.4 could barely kill cells as it was only 14% (Fig. 5b). In addition, cytotoxicity of hydrogels in different culture periods was investigated in a weakly acidic cell culture medium at pH 6.8 to mimic tumor tissues (Fig. 6b). After 24 h, 24% and 27%of Dox was released from the NCQDs/Dox and NCQDs/Dox/HA hydrogel at 6.5 pH (Fig. 5), respectively. As shown in Fig. 6b, 25% of cells cultured with NCQDs/Dox and NCQDs/Dox/HA were significantly inhibited compared to the control, and cell viability showed no significant difference after 24 h. After 48 h, around 26% and 37% of Dox was released from the NCQDs/Dox and NCQDs/Dox/HA hydrogel at 6.5 pH (Fig. 5), respectively. Cell viability decreased from 63% for the NCQDs/Dox to 48% for the NCQDs/Dox/HA. A similar situation was observed after 72 h and the difference between the cell inhibition rates of the two hydrogels increased. After 72 h, both hydrogel groups effectively reduced the number of cells, especially after 3 days of incubation, the cell viability for the NCQD/Dox/HA hydrogel group decreased from 69% to 29%. As shown in Fig. 6b, from day 1 to day 3, MCF-7 cultured with NCQDs/Dox/HA hydrogel groups performed the highest cell inhibition after the pure Dox. Compared to the recent study [52], the increase in the concentration of Dox reduced viability in cancer cells, but in the current study, the effectiveness of the NCQDs/Dox/HA obtained in cancer cells has increased significantly and no similar composite used for this purpose has been found in the literature. The increase in the difference between the cell viability of the NCQDs/Dox and NCQDs/Dox/HA hydrogels was in line with the previous results in current study and, as mentioned earlier, indicated that Dox release increased in acidic medium.

The cell viability in a neutral and weakly acidic environment was also qualitatively assessed by live/dead staining as shown in Fig. 6c and d, respectively. While the viability of MCF-7 treated with NCQD/Dox/HA in neutral culture medium was >99% after one day culture (Fig. 6c), a large part of the image in the acidic culture medium (Fig. 6d) showed red colour representing dead cells, which was consistent with MTT results and indicated that most MCF-7 cells were dead at pH 6.5. While NCQDs/Dox/HA hydrogel groups at pH 7.4 showed large amounts of green live cells, the number of red dead cells increased at pH 6.5. Considering the data in Fig. 5-6, developed NCQD/Dox/HA hydrogels were almost non-toxic to cells in a neutral physiological environment, while demonstrating an excellent capacity for cell inhibition in a tumor-like environment, showing that it was highly sensitive to pH.

To date, in the literature, there is no study about the comparison of the drug release percentage both at neutral and acidic pH and also cell viability percentage both on normal cells and cancer cells of pH sensitive Dox carried smart drug delivery systems. Thus, earlier reported studies including different drug delivery systems were compared with this study for antibacterial, injectability, drug release percentage both at neutral and acidic pH and also cell viability percentage. In the Table 1, it was seen that the cell viability on normal cell of NCQDs was similar to previous related studies. However, according to the current study, the cell viability on cancer cell was quite low compared to similar related studies. The system obtained in this study was also antibacterial and

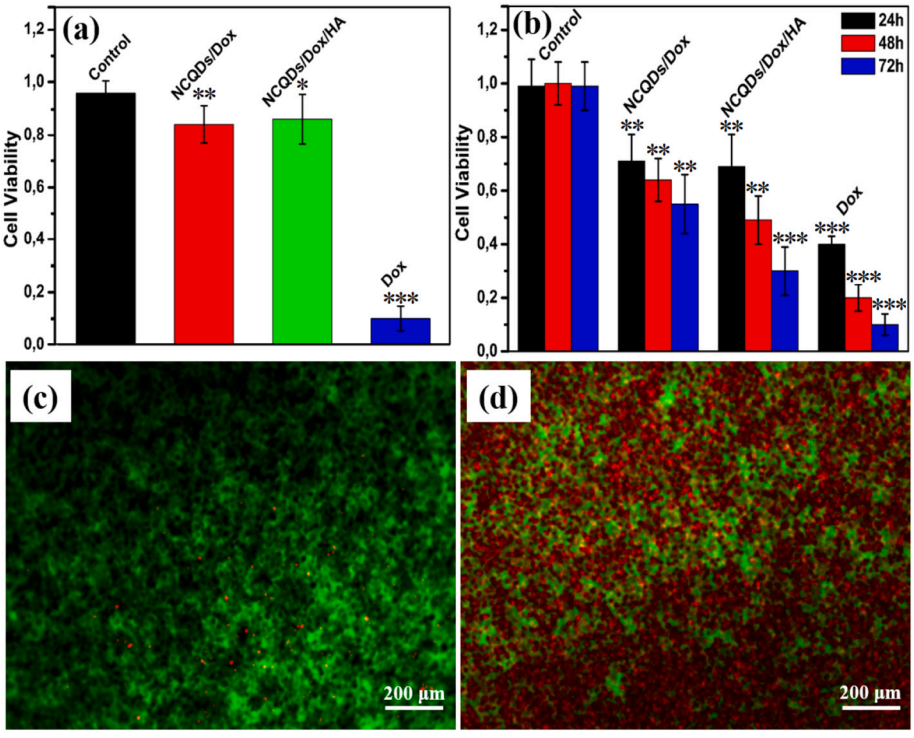

Fig. 6. Cell viability of MCF-7 cells (via MTT method) at (a) pH 7.4 for 24 h, and (b) pH 6.5 for 24 h (black), 48 h (red) and 72 h (blue) (n = 5); (c–d) live/dead assay of MCF-7 cells cultured NCQDs/Dox/HA (0.6/0.2/0.2 wt/vol) for 24 h at (c) pH 7.4 and (d) pH 6.5. Significant differences between control group and treated groups at $*p < 0.05$, $**p < 0.01$, and $***p < 0.001$ are indicated. (For interpretation of the references to colour in this figure legend, the reader is referred to the web version of this article.)

Table 1
Comparison and summary of pH sensitive and Dox carried smart drug delivery systems in the some recent literature.

Compound	Released Drug	Antibacterial	Injectable	Drug release, %		Cell viability, %		Reference
				At neutral pH	At acidic pH	On normal cells	On cancer cells	
Dox/HA/FA	Dox	No	No	~20	~82	~90–100	~45–50	[57]
Zn-HA/Dox	Dox	No	No	~14	~66	~90–100	–	[58]
FA/CH/GOQD/Dox	Dox	No	No	~10	~60	~25–90	~40–70	[48]
Dox/SrHA	Dox	No	No	~20	~23	–	~50–60	[50]
NHA-Gd/Dox	Dox	No	No	~25	~65	~80–90	~25–40	[51]
Dox/Glut/Gly/HA	Dox	No	No	~8	~48	~90–100	–	[59]
mPEG/PCL/Imi/Dox	Dox	No	No	~20	~60	~90–100	~50–60	[60]
NCQDs/Dox/HA	Dox	Yes	Yes	~10	~80	~90–100	~30–40	Present study

injectable, and the drug release in neutral pH was low while the drug release in the acidic environment was higher compared to other studies.

Biomedical imaging application of synthesized NCQDs was evaluated on both breast cancer cells (MCF-7) as a cancer cell model and mouse fibroblast cells (L929) as a normal cell model. The viability of L929 and MCF-7 cells was examined after mixing with 0–500 μgmL^{-1} NCQDs (25, 100, 200, 400, 500 μg mL^{-1}). NCQD cytotoxicity was performed using MTT analysis, and as it can be seen from the results calculated in Fig. 7a, almost 100% viability was observed by incubating L929 or MCF-7 cells with NCQDs for 24 h, even at high NCQD concentrations such as 500 μg mL^{-1}. A previous study observed a similar response, in which cell viability was investigated using Hela cell [53], but it has not been studied as a smart drug delivery system. This results obtained in the current study indicated that NCQDs had a low cytotoxicity and good biocompatibility and confirmed the non-toxic nature of NCQDs, which also meant that NCQDs can potentially be used in biological applications such as drug delivery and bioimaging.

Moreover, the multicolor bio-imaging potentials of NCQDs were investigated using a confocal fluorescence microscope by in vitro bioimaging study after incubation of NCQDs (1 μg mL^{-1}) with L929 and MCF-7 cells for 1 h at 37 °C. The onset of stimulation of MCF-7 cells showed excellent green, blue and less red fluorescence (Fig. 7b), thus differentiating staining of cells was highly visible in MCF-7 cells, possibly due to high cellular uptake and metabolism in cancer cells [54]. The red fluorescence was completely faded and less fluorescent imaging potential was found in the L929 compared to other cancer cell lines. In addition, while L929 cells exhibited less fluorescent images on the blue filter, reasonable images were obtained upon treatment. These results were in agreement with the previous study [55], but no study has yet been conducted on L929 and MCF-7. The NCQDs synthesized in the current study performed fluorescent properties (in blue, green, red filters) on L929 and MCF-7 and were also potential bioimaging agents for in vivo imaging.

The in vitro cytotoxicity of hydrogels with different concentrations of drugs and HA has been investigated qualitatively with a live/dead assay as shown in Fig. 11a, where few dead cells have appeared in all hydrogels due to cell metabolism and apoptosis. After incubation with different drug and HA content hydrogels for 6 h, most of the cells in the hydrogels showed green fluorescence and it was demonstrated that changing the amount of Dox or HA did not affect cytotoxicity of NCQDs based hydrogels at applied compositions.

As shown in Fig. 8b, cell viability of the NCQD-based hydrogels with HA or Dox concentration modified was not affected, and no major change in cell viability was observed when compared to each of the

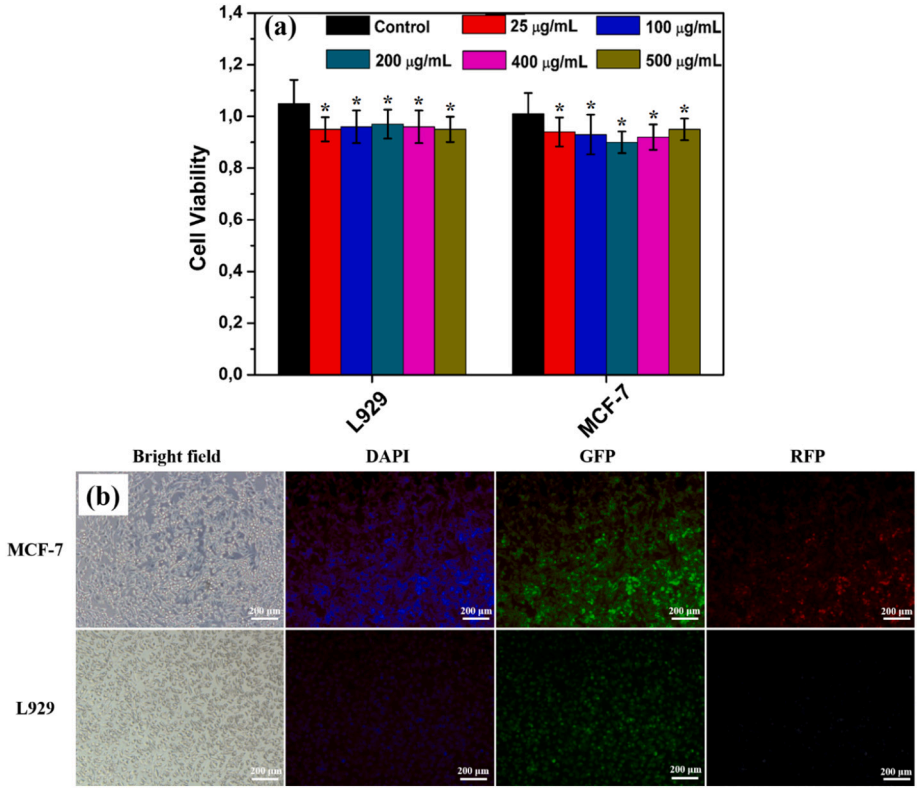

Fig. 7. (a) Effect of the concentration of NCQDs (25, 100, 200, 400, 500 μg/mL) on the viability of L929, and MCF-7 cells (via MTT method) after 24-h incubation (n = 3). (b) The multicolor biolabeling potential of NCQDs (1μg/mL) cultured in L929, and MCF-7 cell lines for 1 h displays DAPI (Blue), GFP (Green), and RFP (Red). *$p < 0.05$, comparison between control group and other groups. (For interpretation of the references to colour in this figure legend, the reader is referred to the web version of this article.)

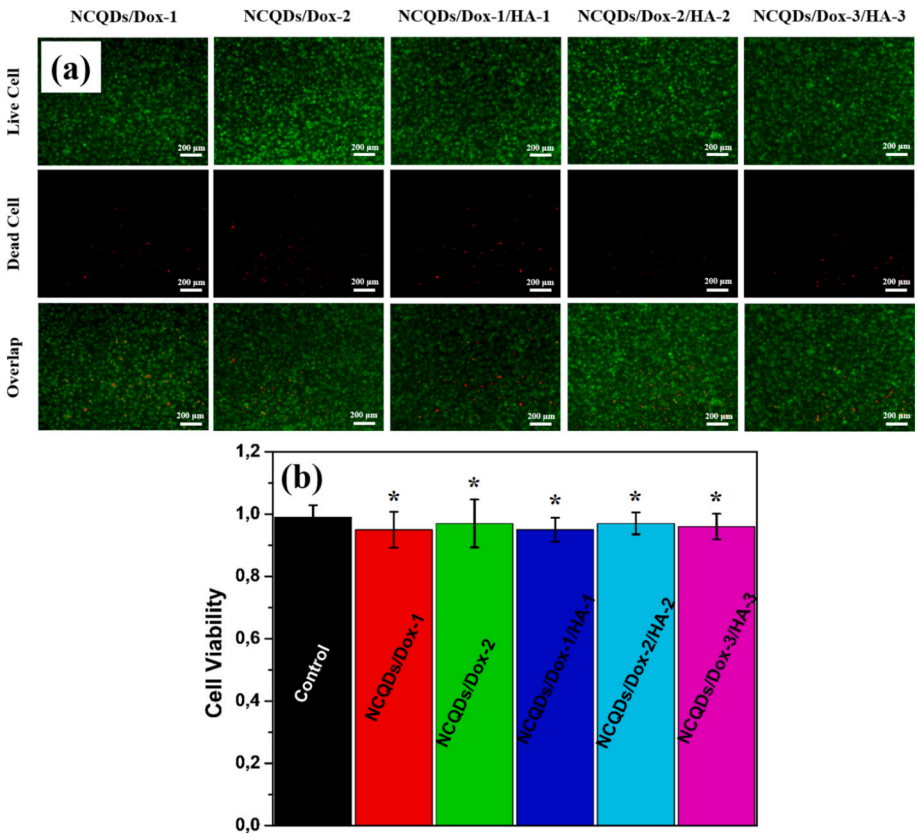

Fig. 8. (a) Fluorescence images of L929 cells after the incubation with NCQDs/Dox-1 (0.6/0.1 wt/vol), NCQDs/Dox-2 (0.6/0.2 wt/vol), NCQDs/Dox-1/HA-1 (0.6/0.1/0.1 wt/vol), NCQDs/Dox-2/HA-2 (0.6/0.2/0.2 wt/vol) and NCQDs/Dox-3/HA-3 (0.6/0.4/0.4 wt/vol) in dark at 37 °C. (b) The cell viability of NCQDs/Dox-1 (0.6/0.1 wt/vol), NCQDs/Dox-2 (0.6/0.2 wt/vol), NCQDs/Dox-1/HA-1 (0.6/0.1/0.1 wt/vol), NCQDs/Dox-2/HA-2 (0.6/0.2/0.2 wt/vol) and NCQDs/Dox-3/HA-3 (0.6/0.4/0.4 wt/vol) after the incubation measured by MTT method. Mean for n = 3 ± SD. *$p < 0.05$, comparison between control group and other groups.

hydrogel groups. In addition, cell viability exhibited over 95% for NCQDs/Dox/HA hydrogels groups with varying contents of Dox and HA which did not show cytotoxicity in good agreement with the live/dead assay. Compared to the recently reported injectable HA-based composite study [56], HA was known to have a certain viability within the hybrid and in the present study, an injectable high cell viability hybrid with increased HA concentration was obtained. These results obtained in the current study suggested that HA or Dox have no effect on cell viability. Both cell viability and live/dead staining results revealed that hydrogels have good cytocompatibility as an intelligent drug delivery system.

4. Conclusion

In this paper, we have successfully developed a novel injectable pH sensitive NCQDs/Dox/HA hydrogel smart drug delivery system to efficiently deliver Dox into the target tumor cells. This self-crosslinking hydrogel was in situ fabricated at physiological conditions via the combination of Schiff base, ionic and H- bond interactions among the three components of the hydrogel. The resulting injectable and covalent NCQDs based hydrogel with bioactive HA successfully demonstrated the in-situ gelation and therefore had a suitable injectability at the body temperature. The acidic sensitivity of the Schiff base and HA components led to a highly sensitive drug release profile at different pH values from Dox conjugated hydrogels, which was verified by MTT assay, UV–Vis spectrometry, live/dead assay, and florescent microscope images. Our results suggested that the binding mechanism for NCQDs-Dox for the most appropriate smart drug delivery systems can lead to the new approach. The injectable smart drug delivery hydrogel were synthesized through the Schiff base reaction between NCQDs−Dox and ionic interactions between NCQDs−HA and Dox−HA, suggesting a novel method to load drugs in NCQDs based hybrid hydrogel. NCQDs/Dox/HA exhibited effective time and pH-dependent drug release in cell mimic environment which is beneficial for chemotherapy due to reduces the side effect of the cancer drugs in normal tissues and relatively low pH in cancerous tissues. Moreover, it was demonstrated that the NCQDs/Dox/HA hybrids exhibited potent antibacterial activity against *S. aureus* in vitro. The in vitro efficacy and cytotoxic of Dox released from nano engineered injectable hydrogels was also examined with L929 and MCF-7 cells and no cytotoxic effect of the hydrogels was observed. The hydrogels were non-toxic to MCF-7 cells at natural pH, and Dox released from NCQDs/Dox/HA hydrogel induced cell death effectively at acidic pH. In addition, a higher therapeutic effect in MCF-7 tumor cells was achieved by more efficient intracellular delivery of Dox by NCQDs/Dox/HA, which showed good potential as a smart drug delivery system.

This study, which can be applied in the field of cancer in the future, will provide convenience in invasive cancer applications thanks to its adjustable gelling time and injectability. In addition, the current study is a multi-functional study that not only increases drug release to the cancerous area thanks to its pH sensitivity, but also prevents bacterial infection that can be transmitted from the application environment thanks to antibacterial activity and has remarkable benefits to be applied in the field of cancer.

There are no previous reports with NCQDs based pH sensitive and injectable NCQDs/Dox/HA hydrogel smart drug delivery systems tested as drug nanocarriers or/and for the delivery of Dox in open literature. Overall, these results showed that injectable pH sensitive intelligent nano-engineered NCQDs/Dox/HA hydrogels were a promising nano-therapeutic agent for antitumor treatment in vivo, which will be carried out by our team as the next step, since these hydrogels offered a new teraconic window and may be included in future clinical practice for a better quality of life.

Declaration of competing interest

The authors declare that they have no known competing financial interests or personal relationships that could have appeared to influence

the work reported in this paper.

Acknowledgments

We thank the staff of BIMAS-RC for insightful and helpful discussions. This work is supported by the Scientific Research Projects Commission of Sakarya University (Project number: 2019-5-19-26, 2019-6-23-223).

Appendix A. Supplementary data

Supplementary data to this article can be found online at https://doi.org/10.1016/j.msec.2020.111829.

References

[1] H.H. Kyu, D. Abate, K.H. Abate, E. Al, Global, regional, and national disability-adjusted life-years (DALYs) for 359 diseases and injuries and healthy life expectancy (HALE) for 195 countries and territories, 1990–2017: A systematic analysis for the Global Burden of Disease Study 2017, Lancet. 392 (2018) 1859–1922, https://doi.org/10.1016/S0140-6736(18)32335-3.

[2] Y. Li, E. Kumacheva, Hydrogel microenvironments for cancer spheroid growth and drug screening, Sci. Adv. 4 (2018) 1–11, https://doi.org/10.1126/sciadv.aas8998.

[3] S. Niu, G.R. Williams, J. Wu, J. Wu, X. Zhang, H. Zheng, S. Li, L.M. Zhu, A novel chitosan-based nanomedicine for multi-drug resistant breast cancer therapy, Chem. Eng. J. 369 (2019) 134–149, https://doi.org/10.1016/j.cej.2019.02.201.

[4] E. Tasca, A. Del Giudice, L. Galantini, K. Schillén, A.M. Giuliani, M. Giustini, A fluorescence study of the loading and time stability of doxorubicin in sodium cholate/PEO-PPO-PEO triblock copolymer mixed micelles, J. Colloid Interface Sci. 540 (2019) 593–601, https://doi.org/10.1016/j.jcis.2019.01.075.

[5] X.Y. Wong, A. Sena-Torralba, R. Alvarez-Diduk, K. Muthoosamy, A. Merkoçi, et al., ACS Nano. (2020) 1–256, https://doi.org/10.1021/acsnano.9b08133. February.

[6] E. Tasca, P. Andreozzi, A. del Giudice, L. Galantini Funding, K. Schillén, A. Maria Giuliani, M. de los Angeles Ramirez, S. Moya, M. Giustini, Poloxamer/sodium cholate co-formulation for micellar encapsulation of Doxorubicin with high efficiency for intracellular delivery: an in-vitro bioavailability study, J. Colloid Interface Sci. 579 (2020) 551–561, https://doi.org/10.1016/j.jcis.2020.06.096.

[7] Q. Jia, Z. Li, C. Guo, X. Huang, M. Kang, Y. Song, L. He, N. Zhou, M. Wang, Z. Zhang, G. Fu, M. Du, PEGMA-modified bimetallic NiCo Prussian blue analogue doped with Tb(III) ions: Efficiently pH-responsive and controlled release system for anticancer drug, Chem. Eng. J. 389 (2020), https://doi.org/10.1016/j.cej.2020.124468, 124468.

[8] G. Guan, M. Wu, M.Y. Han, Stimuli-responsive hybridized nanostructures, Adv. Funct. Mater. 30 (2020) 1–27, https://doi.org/10.1002/adfm.201903439.

[9] X. Yuan, S. Peng, W. Lin, J. Wang, L. Zhang, Multistage pH-responsive mesoporous silica nanohybrids with charge reversal and intracellular release for efficient anticancer drug delivery, J. Colloid Interface Sci. 555 (2019) 82–93, https://doi.org/10.1016/j.jcis.2019.07.061.

[10] W.H. Chen, G.F. Luo, X.Z. Zhang, Recent advances in subcellular targeted cancer therapy based on functional materials, Adv. Mater. 31 (2019) 1–39, https://doi.org/10.1002/adma.201802725.

[11] G. Bin Qi, Y.J. Gao, L. Wang, H. Wang, Self-assembled peptide-based nanomaterials for biomedical imaging and therapy, Adv. Mater. 30 (2018), https://doi.org/10.1002/adma.201703444.

[12] Y. Ma, L. Shi, F. Liu, Y. Zhang, Y. Pang, X. Shen, Self-assembled thixotropic silver cluster hydrogel for anticancer drug release, Chem. Eng. J. 362 (2019) 650–657, https://doi.org/10.1016/j.cej.2019.01.096.

[13] Q. Jia, Z. Zhao, K. Liang, F. Nan, Y. Li, J. Wang, J. Ge, P. Wang, Recent advances and prospects of carbon dots in cancer nanotheranostics, Mater. Chem. Front. 4 (2020) 449–471, https://doi.org/10.1039/c9qm00667b.

[14] K. Dehvari, S.-H. Chiu, J.-S. Lin, W.M. Girm, Y.-C. Ling, J.-Y. Chang, Heteroatom doped carbon dots with nanoenzyme like properties as theranostic platforms for free radical scavenging, imaging, and chemotherapy, Biomaterialia. (2020), https://doi.org/10.2139/ssrn.3527826.

[15] X. Yuan, J. Zhang, M. Yan, M. Si, L. Jiang, Y. Li, H. Yu, J. Zhang, G. Zeng, Nitrogen doped carbon quantum dots promoted the construction of Z-scheme system with enhanced molecular oxygen activation ability, J. Colloid Interface Sci. 541 (2019) 123–132, https://doi.org/10.1016/j.jcis.2019.01.072.

[16] W. Su, H. Wu, H. Xu, Y. Zhang, Y. Li, X. Li, L. Fan, Carbon dots: a booming material for biomedical applications, Mater. Chem. Front. 4 (2020) 821–836, https://doi.org/10.1039/c9qm00658c.

[17] Z. Wang, J. Chen, L. Wang, G. Gao, Y. Zhou, R. Wang, T. Xu, J. Yin, J. Fu, Flexible and wearable strain sensors based on tough and self-adhesive ion conducting hydrogels, J. Mater. Chem. B. 7 (2019) 24–29, https://doi.org/10.1039/c8tb02629g.

[18] Y. Yan, F. Qi, S. Zhao, Y. Luo, S. Gu, Q. Li, L. Zhang, S. Zhou, N. Bolan, A new low-cost hydroxyapatite for efficient immobilization of lead, J. Colloid Interface Sci. 553 (2019) 798–804, https://doi.org/10.1016/j.jcis.2019.06.090.

[19] S. Ferraris, S. Yamaguchi, N. Barbani, M. Cazzola, C. Cristallini, M. Miola, E. Vernè, S. Spriano, Bioactive materials: in vitro investigation of different mechanisms of hydroxyapatite precipitation, Biomaterialia. 102 (2020) 468–480, https://doi.org/10.1016/j.actbio.2019.11.024.

[20] Y. Liu, Y. Tang, J. Wu, J. Sun, X. Liao, Z. Teng, G. Lu, Facile synthesis of biodegradable flower-like hydroxyapatite for drug and gene delivery, J. Colloid Interface Sci. 570 (2020) 402–410. doi:https://doi.org/10.1016/j.jcis.2020.03.010.

[21] Y. Hu, S. Cao, J. Chen, Y. Zhao, F. He, Q. Li, L. Zou, C. Shi, Biomimetic fabrication of icariin loaded nano hydroxyapatite reinforced bioactive porous scaffolds for bone regeneration, Chem. Eng. J. 394 (2020), https://doi.org/10.1016/j.cej.2020.124895, 124895.

[22] C. Zhao, X. Wang, L. Wu, W. Wu, Y. Zheng, L. Lin, Nitrogen-doped carbon quantum dots as an antimicrobial agent against Staphylococcus for the treatment of infected wounds, Colloids Surfaces B Biointerfaces. 179 (2019) 17–27, https://doi.org/10.1016/j.colsurfb.2019.03.042.

[23] R. Riaz, M. Ali, T. Maiyalagan, A. Sameen, S. Lee, M. Jae, Dye-sensitized solar cell (DSSC) coated with energy down shift layer of nitrogen-doped carbon quantum dots (N-CQDs) for enhanced current density and stability Applied Surface Science Dye-sensitized solar cell (DSSC) coated with energy down shift lay, Appl. Surf. Sci. 483 (2019) 425–431, https://doi.org/10.1016/j.apsusc.2019.03.236.

[24] X. Lu, C. Liu, Z. Wang, J. Yang, M. Xu, J. Dong, P. Wang, Nitrogen-doped carbon nanoparticles derived from silkworm excrement as on–off–on fluorescent sensors to detect Fe (III) and biothiols, Nanomaterials. 8 (2018) 1–12, https://doi.org/10.3390/nano8060443.

[25] M. Fan, Y. Ma, H. Tan, Y. Jia, S. Zou, S. Guo, M. Zhao, H. Huang, Z. Ling, Y. Chen, X. Hu, Covalent and injectable chitosan-chondroitin sulfate hydrogels embedded with chitosan microspheres for drug delivery and tissue engineering, Mater. Sci. Eng. C. 71 (2017) 67–74, https://doi.org/10.1016/j.msec.2016.09.068.

[26] S. Türk, I. Altınsoy, G.Ç. Efe, M. Ipek, M. Özacar, C. Bindal, Biomimetic synthesis of Ag, Zn or Co doped HA and coating of Ag, Zn or Co doped HA/f MWCNT composite on functionalized Ti, Mater. Sci. Eng. C. 99 (2019) 986–998, https://doi.org/10.1016/j.msec.2019.02.025.

[27] X. Liu, J. Liu, B. Zheng, L. Yan, J. Dai, Z. Zhuang, J. Du, Y. Guo, D. Xiao, N-Doped carbon dots: green and efficient synthesis on a large-scale and their application in fluorescent pH sensing, New J. Chem. 41 (2017) 10607–10612, https://doi.org/10.1039/c7nj01889d.

[28] J. Tan, R. Zou, J. Zhang, W. Li, L. Zhang, D. Yue, Large-scale synthesis of N-doped carbon quantum dots and their phosphorescence properties in a polyurethane matrix, Nanoscale. 8 (2016) 4742–4747, https://doi.org/10.1039/c5nr08516k.

[29] Z. Wang, L. Cao, Y. Ding, R. Shi, X. Wang, H. Lu, Z. Liu, F. Xiu, J. Liu, W. Huang, One-step and green synthesis of nitrogen-doped carbon quantum dots for multifunctional electronics, RSC Adv. 7 (2017) 21969–21973. doi:https://doi.org/10.1039/c7ra03840b.

[30] D.C. Manatunga, R.M. De Silva, K.M.N. De Silva, D.T. Wijeratne, G.N. Malavige, G. Williams, Fabrication of 6-gingerol , doxorubicin and alginate hydroxyapatite into a bio - compatible formulation : enhanced anti - proliferative effect on breast and liver cancer cells, Chem. Cent. J. 12 (2018) 1–13.

[31] G. Bharath, A. Naldoni, K.H. Ramsait, A. Abdel-wahab, Enhanced electrocatalytic activity of gold nanoparticles on hydroxyapatite nanorods for sensitive hydrazine sensors, J. Mater. Chem. A 4 (2016) 6385–6394, https://doi.org/10.1039/c6ta01528j.

[32] C.C. Negrila, M.V. Predoi, S.L. Iconaru, D. Predoi, Development of zinc-doped hydroxyapatite by sol-gel method for medical applications, Molecules. 23 (2018) 1–15, https://doi.org/10.3390/molecules23112986.

[33] T. Li, X. Song, C. Weng, X. Wang, L. Sun, X. Gong, L. Yang, C. Chen, et al., Appl. Mater. Today. 10 (2018) 173–183, https://doi.org/10.1016/j.apmt.2017.12.002.

[34] C. Rizzo, F. Arcudi, Đ. Luka, N.T. Dintcheva, R. Noto, F.D. Anna, M. Prato, Nitrogen-doped carbon nanodots-ionogels: preparation, characterization, and radical scavenging activity, ACS Nano. 12 (2018) 1296–1305, https://doi.org/10.1021/acsnano.7b07529.

[35] B. Ren, X. Chen, S. Du, Y. Ma, H. Chen, G. Yuan, J. Li, D. Xiong, H. Tan, Z. Ling, Y. Chen, X. Hu, X. Niu, Injectable polysaccharide hydrogel embedded with hydroxyapatite and calcium carbonate for drug delivery and bone tissue engineering, Int. J. Biol. Macromol. 118 (2018) 1257–1266, https://doi.org/10.1016/j.ijbiomac.2018.06.200.

[36] L. Wang, F. Deng, W. Wang, A. Li, C. Lu, H. Chen, G. Wu, K. Nan, L. Li, Construction of injectable self-healing macroporous hydrogels via a template-free method for tissue engineering and drug delivery, ACS Appl. Mater. Interfaces. 10 (2018) 36721–36732, https://doi.org/10.1021/acsami.8b13077.

[37] C. Lan, S. Zhao, Self-assembled nanomaterials for synergistic antitumour therapy, J. Mater. Chem. B. 6 (2018) 6685–6704, https://doi.org/10.1039/c8tb01978a.

[38] N.M. Morsi, R. Nabil Shamma, N. Osama Eladawy, A.A. Abdelkhalek, Bioactive injectable triple acting thermosensitive hydrogel enriched with nano-hydroxyapatite for bone regeneration: in-vitro characterization, Saos-2 cell line cell viability and osteogenic markers evaluation, Drug Dev. Ind. Pharm. 45 (2019) 787–804, https://doi.org/10.1080/03639045.2019.1572184.

[39] S. Yan, J. Ren, Y. Jian, W. Wang, W. Yun, J. Yin, Injectable maltodextrin based micelle/hydrogel composites for simvastatin controlled release, Biomacromolecules. 19 (2018) 4554–4564, https://doi.org/10.1021/acs.biomac.8b01234.

[40] H.C.W. Parks, T.M. Mccoy, R.F. Tabor, Carbon quantum dot assisted adsorption of graphene oxide to the oil – water interface for copper sensing emulsions, Adv. Mater. Interfaces. 6 (2019) 1–10, https://doi.org/10.1002/admi.201900392.

[41] S.E.F. Marques, J.B. Nieder, Surface charge tunable catanionic vesicles based on serine-derived surfactants as efficient nanocarriers for the delivery of the anticancer drug doxorubicin, Nanoscale. 11 (2019) 5932–5941, https://doi.org/10.1039/c8nr06346j.

[42] N. Song, A. Wang, Study on influencing factors of Pickering emulsions stabilized by hydroxyapatite nanoparticles with nonionic surfactants, Soft Matter. 14 (2018) 3889–3901, https://doi.org/10.1039/c8sm00241j.
[43] M. Charlotte, E. Laurichesse, A. Perro, V. Ravaine, V. Schmitt, Kinetics of spontaneous microgels adsorption and stabilization of emulsions produced using microfluidics, J. Colloid Interface Sci. 548 (2019) 1–11, https://doi.org/10.1016/j.jcis.2019.04.020.
[44] A. Gupta, S. Mumtaz, C.H. Li, I. Hussain, V.M. Rotello, Combatting antibiotic-resistant bacteria using nanomaterials, Chem. Soc. Rev. 48 (2019) 415–427, https://doi.org/10.1039/c7cs00748e.
[45] J.D. Caplin, A.J. García, Implantable antimicrobial biomaterials for local drug delivery in bone infection models, Acta Biomater. 93 (2019) 2–11, https://doi.org/10.1016/j.actbio.2019.01.015.
[46] T. Shen, W. Yang, X. Shen, W. Chen, B. Tao, X. Yang, J. Yuan, P. Liu, K. Cai, Polydopamine-assisted hydroxyapatite and lactoferrin multilayer on titanium for regulating bone balance and enhancing antibacterial property, ACS Biomater. Sci. Eng. 4 (2018) 3211–3223, https://doi.org/10.1021/acsbiomaterials.8b00791.
[47] R. Jijie, A. Barras, J. Bouckaert, N. Dumitrascu, S. Szunerits, Enhanced antibacterial activity of carbon dots functionalized with ampicillin combined with visible light triggered photodynamic effects, Colloids Surfaces B Biointerfaces. 170 (2018) 347–354, https://doi.org/10.1016/j.colsurfb.2018.06.040.
[48] S. De, K. Patra, D. Ghosh, K. Dutta, A. Dey, G. Sarkar, J. Maiti, A. Basu, D. Rana, D. Chattopadhyay, Tailoring the efficacy of multifunctional biopolymeric graphene oxide quantum dot-based nanomaterial as nanocargo in cancer therapeutic application, ACS Biomater. Sci. Eng. 4 (2018) 514–531, https://doi.org/10.1021/acsbiomaterials.7b00689.
[49] M.U. Munir, A. Ihsan, Y. Sarwar, S.Z. Bajwa, K. Bano, B. Tehseen, N. Zeb, I. Hussain, M.T. Ansari, M. Saeed, J. Li, M.Z. Iqbal, A. Wu, W.S. Khan, Hollow mesoporous hydroxyapatite nanostructures; smart nanocarriers with high drug loading and controlled releasing features, Int. J. Pharm. 544 (2018) 112–120, https://doi.org/10.1016/j.ijpharm.2018.04.029.
[50] S. Agrawal, M. Kelkar, A. De, Newly emerging mesoporous strontium hydroxyapatite nanorods: microwave synthesis and relevance as doxorubicin nanocarrier, J Nanopart Res. 20 (2018) 1–11.
[51] Y. Tang, G. Lu, J. Wu, Y. Liu, S. Wang, J. Sun, Z. Teng, Y. Tian, Gadolinium-doped hydroxyapatite nanorods as t1 contrast agents and drug carriers for breast cancer therapy, ACS Appl. Nano Mater. 2 (2019) 1194–1201, https://doi.org/10.1021/acsanm.8b02036.
[52] A. Srivastava, C. Liu, J. Lv, W. Qiao, Enhanced intercellular release of anticancer drug by using nano-sized catanionic vesicles of doxorubicin hydrochloride and gemini surfactants, J. Mol. Liq. 259 (2018) 398–410, https://doi.org/10.1016/j.molliq.2018.03.065.
[53] V. Singh, S. Kashyap, U. Yadav, A. Srivastava, A.V. Singh, R.K. Singh, S.K. Singh, P. S. Saxena, Nitrogen doped carbon quantum dots demonstrate no toxicity under in vitro conditions in a cervical cell line and in vivo in Swiss albino mice, Toxicol. Res. 8 (2019) 395–406, https://doi.org/10.1039/c8tx00260f.
[54] S.Y. Lim, W. Shen, Z. Gao, Carbon quantum dots and their applications, Chem. Soc. Rev. 44 (2015) 362–381, https://doi.org/10.1039/c4cs00269e.
[55] T. Pal, S. Mohiyuddin, G. Packirisamy, Facile and green synthesis of multicolor fluorescence carbon dots from curcumin: in vitro and in vivo bioimaging and other applications, ACS Omega. 3 (2018) 831–843, https://doi.org/10.1021/acsomega.7b01323.
[56] X. Yang, M.G. Raucci, X. Zhu, M. Santin, L. Ambrosio, B. Yuan, Y. Fan, X. Zhang, Injectable strontium-doped hydroxyapatite integrated with phosphoserine-tethered poly(epsilon-lysine) dendrons for osteoporotic bone defect repair, J. Mater. Chem. B. 6 (2018) 7974–7984, https://doi.org/10.1039/c8tb02526f.
[57] W. Sun, J. Fan, S. Wang, Y. Kang, J. Du, X. Peng, Biodegradable drug-loaded hydroxyapatite nanotherapeutic agent for targeted drug release in tumors, ACS Appl. Mater. Interfaces. 10 (2018) 7832–7840, https://doi.org/10.1021/acsami.7b19281.
[58] H. Kim, S. Mondal, S. Bharathiraja, P. Manivasagan, Optimized Zn-doped hydroxyapatite/doxorubicin bioceramics system for e ffi cient drug delivery and tissue engineering application, Ceram. Int. 44 (2018) 6062–6071, https://doi.org/10.1016/j.ceramint.2017.12.235.
[59] B. Pandey, G. Verma, P. Hassan, N.G. Shetake, K.C. Barick, I.P. Kavirayani, Covalent immobilization of doxorubicin in glycine functionalized hydroxyapatite nanoparticles for pH-responsive release, New J. Chem. 42 (2018) 6283–6292, https://doi.org/10.1039/c7nj04706a.
[60] Y. Zhai, X. Zhou, Z. Zhang, L. Zhang, D. Wang, Design, synthesis, and characterization of schiff base bond-linked ph-responsive doxorubicin prodrug based on functionalized mPEG-PCL for targeted cancer therapy, Polymers (Basel). 10 (2018) 1–12, https://doi.org/10.3390/polym10101127.